Mathematical Biosciences and Engineering

http://www.aimspress.com/journal/MBE

Mathematical Biosciences and Engineering, 16(4): 2795–2810.
DOI: 10.3934/mbe.2019139
Received: 29 December 2018
Accepted: 05 March 2019
Published: 01 April 2019

Research article

Mechano-biological model of glioblastoma cells in response to osmotic stress

Giulia Pozzi[1,†], **Stefano Marchesi**[1,2,†], **Giorgio Scita**[2,3], **Davide Ambrosi**[4] **and Pasquale Ciarletta**[1,*]

[1] MOX Laboratory, Department of Mathematics, Politecnico di Milano, Italy
[2] IFOM, the FIRC Institute of Molecular Oncology, Via Adamello 16, 20139 Milan, Italy
[3] Department of Oncology and Hemato-Oncology, University of Milan, Milan, Italy
[4] DISMA, Dipartimento di Scienze Matematiche "G.L. Lagrange", Politecnico di Torino, Italy

† The authors contributed equally to this work.

* **Correspondence:** Email: pasquale.ciarletta@polimi.it; Tel: +390223994565.

Abstract: This work investigates the mechano-biological features of cells cultured in monolayers in response to different osmotic conditions. *In-vitro* experiments have been performed to quantify the long-term effects of prolonged osmotic stresses on the morphology and proliferation capacity of glioblastoma cells. The experimental results highlight that both hypotonic and hypertonic conditions affect the proliferative rate of glioblastoma cells on different cell cycle phases. Moreover, glioblastoma cells in hypertonic conditions display a flattened and elongated shape. The latter effect is explained using a nonlinear elastic model for the single cell. Due to a crossover between the free energy contributions related to the cytosol and the cytoskeletal fibers, a critical osmotic stress determines a morphological transition from a uniformly compressed to an elongated shape.

Keywords: mechano-biology; cancer model; biomathematics; glioblastoma; osmotic stress

1. Introduction

Glioblastoma (or glioblastoma multiforme, GBM) is the most common and aggressive adult glioma. It has been estimated that it accounts for approximately 15% of all primary brain and central nervous system tumors and, in particular, for 55% of all gliomas, presenting a more than 90% 2-years mortality [1].

The GBM arises from astrocytes, the most abundant category of glial cells and almost half of the cells contained in the brain glia. From a morphological point of view, this kind of cells is characterized by a star-shape and the presence of ramified protrusions. To be more precise, within the GBM group it

is possible to pinpoint two categories on the base of the clinical appearance: the primary and secondary glioblastoma subtypes. A GBM is defined primary (approximately 90%) if it develops rapidly *de novo* in elderly patients, without clinical or histologic evidence of a less malignant precursor lesion; in this case, patients have symptoms less than six months prior to diagnosis. Conversely, a GBM is defined secondary when it progresses from low-grade diffuse astrocytoma or anaplastic astrocytoma and generally it develops in younger patients with signs and/or symptoms for longer than six months and carries a significant better prognosis. Histologically, primary and secondary glioblastomas are indistinguishable, but they differ in their genetic and epigenetic profiles [2].

Nowadays, the current standard protocol for the treatment of GBM is the maximally possible surgery resection of the tumor combined with radiotherapy and/or chemotherapy [2, 3]. Surgical resection is case-specific and depends on the tumor size, shape, proximity to blood vessels and on the brain region importance in terms of life-function. Radiotherapy in some cases has limited effects, since cells may develop the ability to upregulating the DNA double-stranded break repair machinery, making the treatment ineffective [4]. However, in combination with chemotherapy the median survival rates increase up to 26.5% at 24 months, a vast improvement over the 10.4% with radiotherapy alone [5].

Despite the great progress made in the last decades for the development of new imaging techniques for brain tumours and for genetic targeting of adjuvant therapies [5, 6], the survival rate after clinical treatment of GBM has remained substantially unaltered. Notwithstanding, recent experiments on *in-vitro* system models of GBM have shown that the chemo-mechanical feedbacks due to interactions with the tumour microenvironment may play a key role in determining its invasiveness and its highly infiltrative growth.

The most common system model for the avascular growth phase of solid tumours is the Multicellular Tumour Spheroid (MTS) [7–9]. The MTS is a three dimensional aggregate of cancer cells either seeded in agarose gel or floating within a biological medium filled with nutrients. In [10], MTSs were grown within an inert matrix of agarose gel. Thus, the growing MTS is subjected to a mechanical stress due to the external spatial constraint of the matrix, that mimics the peritumoral stroma. It has been found that the apoptosis rate is directly proportional to the matrix stiffness, with a progressive inhibition on the proliferation rate up to growth saturation. Later works were able to quantify how the local distribution of mechanical stress affect the shape of tumor spheroids [11]. A novel approach has been proposed in [12] by immersing a floating MTS into an external medium enriched with a Dextran solution, that exerts an osmotic pressure independent on the size. The results confirmed the inhibiting effect of a compressive stress, the full reversibility to the stress-free growth curve as far as the Dextran is removed from the culture medium. The imposition of a osmotic stress affects the biological activity of the cells, with an external rim of proliferative cells with reduced apoptosis and a central core characterized by the reverse situation [13]. Regarding specifically the human glioblastoma multiforme, in [14] a set of experiments has been performed investigating the growth of U-87MG spheroids. In the free growth case, it has been shown that it is possible to distinguish between a first stages of growth characterized by an exponential/linear behavior and a second saturation phase where the radius reaches a steady value. On the other hand, the compression experiments performed with Dextran have revealed one more time both the inhibitory effect of stress on growth and the reversibility of this phenomenon.

This inhibiting effect of osmotic stress on tumour cells has been also observed in a two-dimensional system model, where cells are cultured either individually or to form a monolayer.

Although MTS give a more realistic representation of the force transmission between neighboring cells in a three-dimensional embedding, the monolayers are easier to handle experimentally, and can be used to investigate the single cell response in terms of morphology, cell cycle and adhesion. Using different osmotic conditions, gross morphological changes were quantified in cancer cells [15]: hyperosmotic media induce cells to have an elliptical and more tapered shape than cells cultured in isotonic conditions. For the hypotonic treatment, cells tend toward a more rounded morphology at late times. A similar behavior was observed in condrocytes exposed to osmotic shock gang, from hypertonic to hypotonic they exhibit a more spherical shape and membrane ruffles reduction [16]. Beyond the morphological observations, the effect of low osmotic pressure (1 kPa) exerted by Dextran on melanoma proliferation, growth and motility has been investigated in [17, 18]. The reported results show that few functional properties of the cells are heavily affected by osmotic pressure: both proliferation and motility are reduced and significant changes in F-actin organization have been observed. These modifications are more evident in primary melanoma cell lines than in the metastatic one and they are supposed to be responsible for the cells elongation. Moreover, several studies have suggested that chemo-mechanical stimuli from the tumor micro–environment are responsible for alteration in the cell cycle. The effect of the hyposmotic condition has been studied on different colonic and pancreatic cell lines [19], highlighting a reversible growth arrest and, in some cases, the accumulation at the G1/S checkpoint of the cell cycle. The mechanism controlling hyperosmotic stress-induced growth arrest, while it is unknown, seemed not to affect the cell cycle in monolayers culture of murine colon cancer cells [20].

In this work, we introduce a mechanical model that may support a deeper understanding of the mechano-biological features of cells cultured in monolayers in response to different osmotic conditions. The article is structured as follows. In Section 2, we describe the experimental method developed to perform *in-vitro* experiments on a GBM cell line. The main results, presented in Section 3, pertain the experimental characterization of the effects of the osmotic stress on the proliferation and the morphology of a cell monolayer. In Chapter 4, we develop a novel mathematical framework that explains the observed morphological transition triggered by a critical osmotic stress. The main results are summarized and discussed in Section 5.

2. Materials and methods

The experiments were performed at IFOM laboratory. A glioblastoma cell line, T98G, was obtained by ATCC (American Type Culture Collection) consortium. Cells were cultured under 37 °C and 5% CO2 in Dulbecco's modified Eagle's medium plus Fetal Bovine Serum (FBS, 10% in volume), L-glutamine (2 mM), Sodium Pyruvate (1 mM), Non-Essential Amino-Acids (1% in volume) and Penicillin/Streptomycin (100 μg/mL).

Dextran-containing mediums were prepared according to [14]. Briefly, high molecular weight purified Dextran (Mw = 100 kDa, from Sigma-Aldrich, code 0918) was dissolved in complete medium at room temperature till full solubilization. To exert 2 and 5 kPa of mechanical stress on cells, Dextran-containing mediums were prepared with a concentration of 32.5 and 55 g/L respectively.

Hypotonic mediums were prepared according to [21]. Briefly, a solution of sterile water + 1 mM CaCl2 + 1 mM MgCl2 + 10% FBS was prepared. To obtain 50% hypotonic mediums, complete medium was diluted 1:1 with the aforementioned solution. To obtain 25% hypotonic solution, complete

medium was diluted 1:1 with 50% hypotonic medium.

At Day 0, T98G cells were seeded in 100-mm cell culture dishes, in 10 mL of complete medium. Around $4 \cdot 10^5$ cells were seeded in each dish. After 8 hours, isotonic medium was replaced by the same amount of Dextran-containing or hypotonic medium. At Day 3 and 6, cells were imaged at 4X magnification using an EVOS-FL bright-field microscope (ThermoFisher Scientific), equipped with a high-sensitivity monochrome camera (1360 x 1024 pixels, 6.45 μm/pixels). Then, cells were detached by tripsinization and counted with a Multisizer 3 Coulter Counter (Beckman Coulter).

To perform cell cycle analysis, collected cells were re–suspended in 0.3 mL of Phosphate-buffered saline (PBS) solution for every million of cells. Fixation was performed by adding 0.7 mL of cold Ethanol (EtOH 100%) for every million of cells, dropwise while vortexing. DNA staining was performed washing cellular pellets once in PBS-BSA solution (1% w/v) and incubating them in 0.5 mL of PI solution (Propidium Iodide, 50 mg/mL in H20, light protected) plus RNAse A (0.25 mg/mL) overnight at 4 °C. Collected cells were analyzed by DNA content with a Attune NxT Acoustic Focusing Cytometer (ThermoFisher). Quantification of cell cycle distribution and apoptosis was performed with FlowJo software.

3. Experimental results

To understand the long-term effects of prolonged mechanical stimulation on the morphology and proliferation capacity of glioblastoma cells, we cultured T98G cells with Dextran-containing or hypotonic medium for 6 days.

The use of Dextran-containing medium is a well-established method to apply an isotropic compression to single cells or multi-cellular spheroids. Indeed, this high-weight biopolymer is not able to penetrate cell membrane, but accumulates at cell surface, thus exerting a mechanical stress [12, 14, 20].

At day 3, the number of cells growing in Dextran mediums (either 2 or 5 kPa) was smaller than in isotonic medium. Moreover, cells showed an elongated morphology and are more dispersed, without the formation of compact clusters. At day 6 the growth defect was even more evident, since the vast majority of living cells are aberrantly flattened with a certain amount of dead cells floating in the dish, see Figure 1. Conversely, cells growing in hypotonic medium (either 25% or 50%) displayed a mild growth defect without appreciable morphological alterations compared to isotonic control, either at day 3 or day 6, see Figure 1.

The resulting growth curves confirmed the observations by bright-field microscope. The treatment with 25% hypotonic medium had no major effect, whereas cells grown in 50% hypotonic medium showed a delay in proliferation compared to control. On the contrary, cells cultured in Dextran-containing medium experienced a strong growth defect, being almost stacked under 5 kPa of mechanical stress, Figure 2.

To further characterize the effect on cell proliferation, we analyzed cell cycle progression of Dextran/hypotonic-treated cells. Prolonged culture in hypotonic medium caused an accumulation in G1 phase, which is likely the cause of the observed growth delay, Figure 2. Instead, Dextran-containing medium induced an initial accumulation in S phase at day 3, later resulting in a G1-phase accumulation at day 6, Figure 2. Moreover, analysis of fractional DNA content (sub-G1 analysis) highlighted that around 30% of cells underwent apoptosis when constantly cultured in

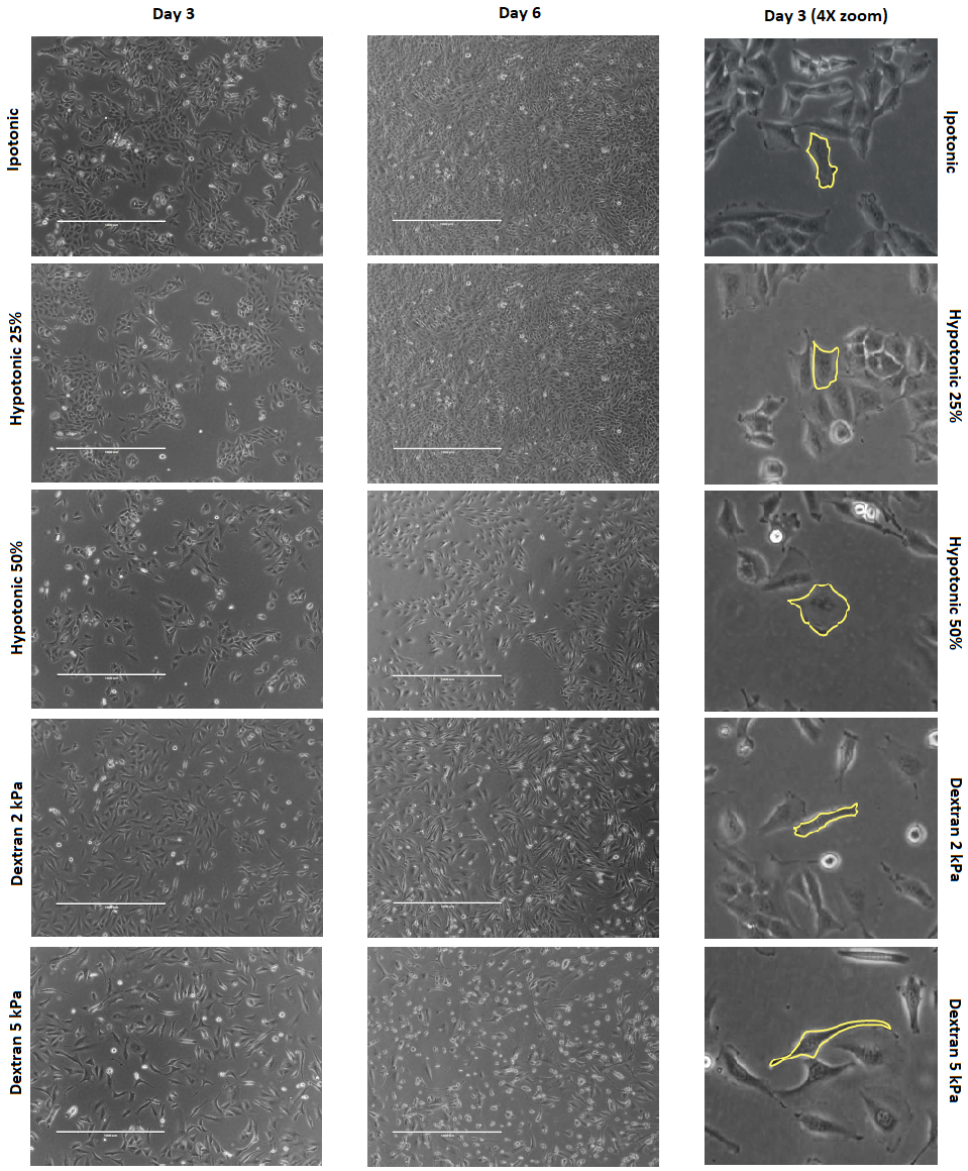

Figure 1. Bright-field microscopy images of T98G cells grown in isotonic, Dextran-containing and hypotonic medium at Day 3 (left), at Day 6 (center), and 4x zoom at Day 3 (right), where the yellow lines depict the cell contours. The white scale bar is 1 mm.

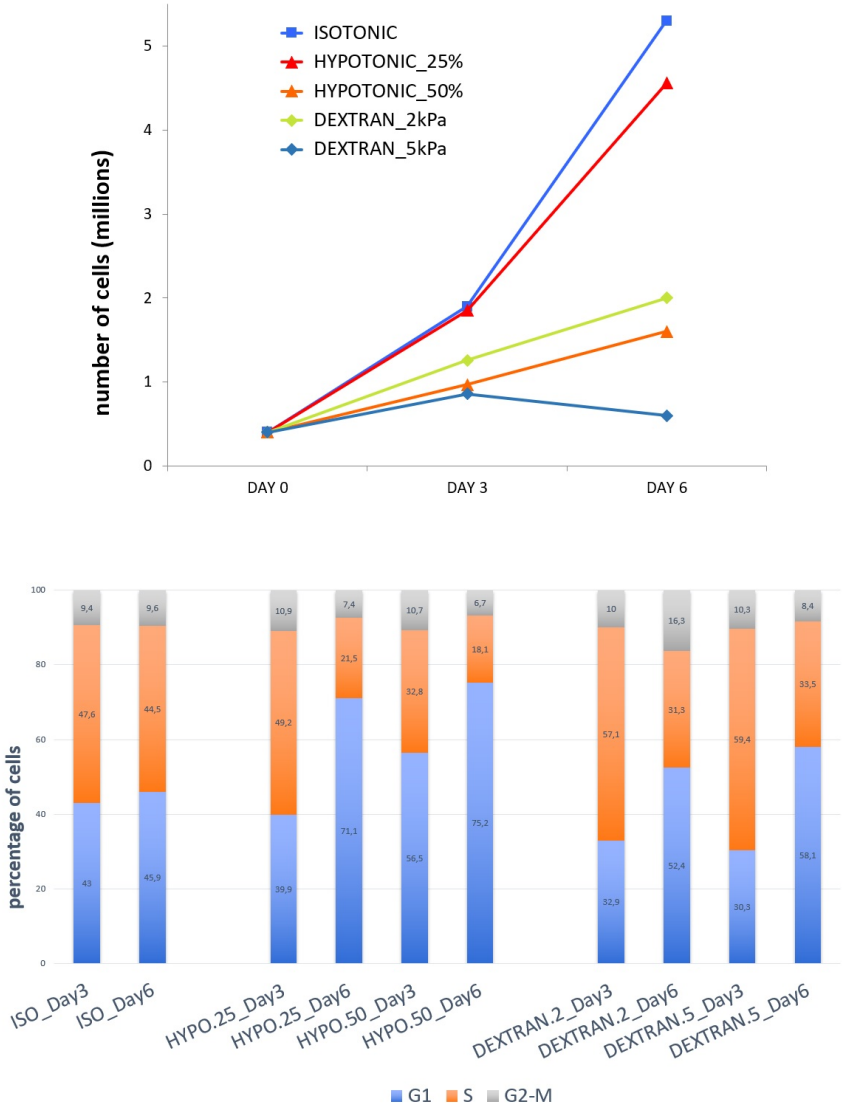

Figure 2. (Top) Growth curves of T98G cells in isotonic, Dextran-containing and hypotonic medium, from day 0 (cell seeding) to day 6. (Bottom) Cell cycle distribution of T98G cells grown in isotonic, Dextran-containing and hypotonic medium, at day 3 and day 6. Collected cells were stained with PI and analyzed for DNA content by flow citometry.

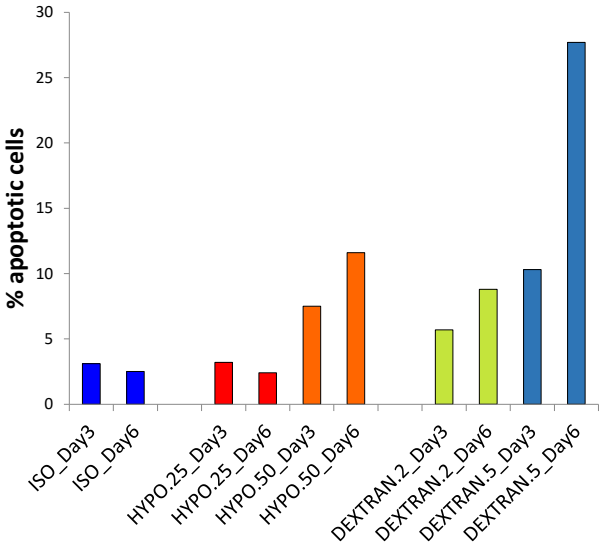

Figure 3. Quantification of apoptotic cells in isotonic, Dextran-containing and hypotonic medium, at day 3 and day 6. Apoptotic cells were measured by sub-G1 analysis of DNA content.

presence of high mechanical stress (5 kPa), Figure 3. These results clearly highlight that prolonged mechanical stimuli impinge on the growth properties of glioblastoma cells on specific cell cycle phases, ultimately limiting the proliferative capacity of tumor cells.

We finally provide a quantitative measurement of the single cell morphology in the different culture conditions. For this purpose we used the Fiji software [22] on the collected images to measure the perimeter p_c and the area A_c for each cell in a sample area of dimension 278 x 252 pixels taken randomly in the central area of the dish. The collected measures allowed to compute an average circularity ratio $\Gamma = 4\pi A_c/p_c^2$, that is depicted in Figure 4.

Notably, we find that there is no statistically significant difference between the morphology of the cells in hypotonic and in isotonic conditions, with a mean circularity value of about $\Gamma = 0.6$. On the contrary, the cells immersed into a hypertonic solution have a significantly lower circularity ratio, with a mean value in the range $\Gamma = 0.25 - 0.35$. Thus, the Dextran molecules are found to trigger a morphological transition towards an elongated shape, that is investigated in the following using a mechanical model.

4. The mathematical model

In this Section we derive a mathematical framework to model the mechano-biological responses observed *in-vitro*, focusing on the morphological changes of a single cell in response to hypertonic conditions.

4.1. The nonlinear elastic boundary value problem

Living cells possess structural and physical properties that enable them to withstand physical forces exerted by the surrounding environment and to adapt themselves to external chemo-mechanical stimuli. At the time scale of interest (days), we can neglect the much faster active dynamics (seconds) of the cytoskeletal units of the cells [23] and the viscoelastic response (minutes) [24]. Thus, we model the adherent GBM cell at equilibrium as a continuous material possessing a solid-like elastic response and an internal microstructure depending on the preferential spatial arrangement of the cytoskeletal fibers.

The cell occupies a portion Ω of the three-dimensional Euclidean space $\mathcal{E}$ in the current configuration, whilst Ω_0 is the reference domain, that is assumed to have a smooth boundary $\partial\Omega_0$.

Let $\mathbf{X}$ and $\mathbf{x}$ be the material and current position vectors, and $\mathbf{e}_i$, $i = 1, 2, 3$ be a orthonormal Cartesian base. The smooth vectorial mapping:

$$\mathbf{x} = \phi(\mathbf{X}),$$

is taken to be twice differentiable, injective except possibly at the boundary $\partial\Omega_0$ and orientation preserving [25], which means that the material cannot penetrate itself or reverse the orientation of material coordinates. We define the *displacement* vector field as:

$$\mathbf{u} = \phi(\mathbf{X}) - \mathbf{X},$$

and the *deformation gradient* tensor as:

$$\mathbf{F}(\mathbf{X}) = \nabla\phi(\mathbf{X}) = \frac{\partial \mathbf{x}}{\partial \mathbf{X}},$$

where the dependence of ϕ on time t drops off because we are at equilibrium.

The single cell is assumed to have a homogeneous mass density per unit volume, thus neglecting the heterogeneity around its cortical layer, and to behave as a perfectly elastic material. Accordingly,

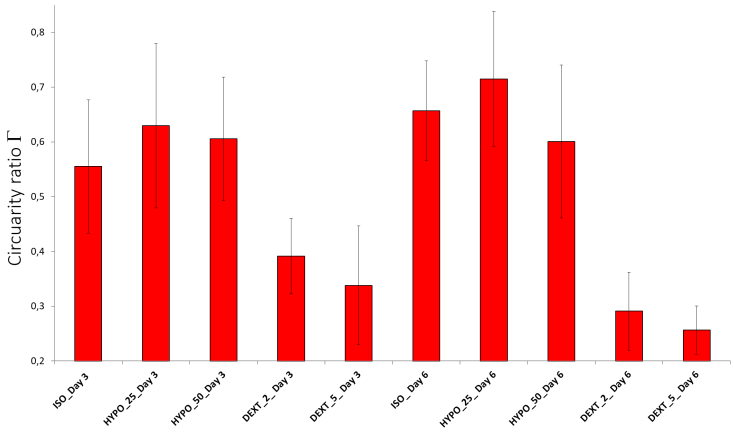

Figure 4. Quantification of mean circularity ratio Γ in isotonic, Dextran-containing and hypotonic medium, at day 3 and day 6. Error bars describe the standard deviation, measuring about 20 cells per sample area.

we define a hyperelastic strain energy function Ψ per unit volume to describe its passive mechanical response, so that the first Piola-Kirchhoff stress tensor $\mathbf{P}$ reads:

$$\mathbf{P} = \frac{\partial \Psi}{\partial \mathbf{F}}. \tag{4.1}$$

In the absence of bulk forces, the balances of linear and angular momentum impose the equation for the elasto–static equilibrium:

$$Div\, \mathbf{P} = 0; \qquad \mathbf{F}\mathbf{P} = \mathbf{P}^T\mathbf{F}; \tag{4.2}$$

where *Div* is the divergence operator material coordinates.
The equilibrium equation is complemented by the following boundary condition at the boundary $\partial\Omega$:

$$\mathbf{P}\mathbf{N}|_{\partial\Omega} = -p_D\, J\mathbf{F}^{-T}\mathbf{N}; \tag{4.3}$$

where $J = \det \mathbf{F}$ is the Jacobian of the mapping, $\mathbf{N}$ is the unit material normal vector, and p_D is the osmotic pressure exerted by the Dextran molecules in the solution.

4.2. Constitutive assumptions and basic solutions

The nonlinear elastic boundary value problem expressed by Eqs (4.2,4.3) can be solved after giving the constitutive law of the strain energy function, that relates the mechanical stress to the local strain within the material.
We assume that the cytoskeletal fibers are mainly oriented along two directions $\mathbf{a}$ and $\mathbf{b}$ in the material configuration, so that the strain energy function is in the form $\Psi = \Psi(\mathbf{F}, \mathbf{a}, \mathbf{b})$. Even though fiber dispersion could be accounted using a more realistic model [26], this simpler assumption contains the minimal ingredients to describe the tensional pattern within the cytoskeleton [27].

By application of the representation theorem of tensor functions [28, 29] to enforce the material symmetry group, this functional dependence can be described with respect to the following invariants:

$$\begin{gathered} I_1 = \mathrm{tr}(\mathbf{F}^T\mathbf{F}), \quad I_2 = \tfrac{1}{2}\left((\mathrm{tr})^2(\mathbf{F}^T\mathbf{F}) - \mathrm{tr}(\mathbf{F}^T\mathbf{F})^2\right), \quad I_3 = \det(\mathbf{F}^T\mathbf{F}) \\ I_4 = (\mathbf{F}\mathbf{a})\cdot(\mathbf{F}\mathbf{a}); \quad I_5 = (\mathbf{F}^T\mathbf{F}\mathbf{a})\cdot(\mathbf{F}^T\mathbf{F}\mathbf{a}); \\ I_6 = (\mathbf{F}\mathbf{b})\cdot(\mathbf{F}\mathbf{b}); \quad I_7 = (\mathbf{F}^T\mathbf{F}\mathbf{b})\cdot(\mathbf{F}^T\mathbf{F}\mathbf{b}); \\ I_8 = (\mathbf{F}\mathbf{a})\cdot(\mathbf{F}\mathbf{b}) \end{gathered} \tag{4.4}$$

We further assume that the anisotropic contributions due to the extensional response of the fibers (expressed by the dependence on the invariants I_4, I_5, I_6, I_7) are negligible with respect to the energy contribution due to the presence of crosslinks in the fiber network, that is encoded in the explicit dependence on I_8. The contour length of the fibers is indeed much bigger than the average distance of fiber entanglement. Thus, the entropic contribution due to the fiber uncrimping is negligible with respect to the enthalpic terms corresponding to the fibers splay. Therefore, we assume the following strain energy function:

$$W(\mathbf{F}, \mathbf{a}, \mathbf{b}) = \frac{\mu_1}{2}\left(I_1 - 3 - \log\left(I_3\right)\right) - \frac{\mu_2}{2}(I_8 - \mathbf{a}\cdot\mathbf{b})^2 \log\left(I_3\right), \tag{4.5}$$

where μ_1 and μ_2 are the material parameters that describe the isotropic and the anisotropic responses, respectively. The energy term multiplying μ_1 describes a compressible neo-Hookean material, that is

the minimal model used to describe the solid stress in tumour cells [30]. The anisotropic contribution contains a novel functional dependence on both I_8 and I_3, mimicking the passive response due to the fiber splay within the cytoskeleton, also affecting the cell compressibility. We remark that in the absence of deformation, i.e. for $\mathbf{F} = \mathbf{I}$, the anisotropic strain measure $(I_8 - \mathbf{a} \cdot \mathbf{b})$ vanishes [31]. By simple application of the chain differentiation rule to Eq (4.5), the first Piola-Kirchhoff stress tensor is given by:

$$\mathbf{P} = \frac{\partial W(\mathbf{F}, \mathbf{a}, \mathbf{b})}{\partial \mathbf{F}} = \mu_1 \mathbf{F} - \Big(\mu_1 + (I_8 - \mathbf{a} \cdot \mathbf{b})^2 \mu_2\Big) \mathbf{F}^{-T} - \frac{\mu_2}{2} \log(I_3)(I_8 - \mathbf{a} \cdot \mathbf{b}) \Big(\mathbf{F}\mathbf{a} \otimes \mathbf{b} + \mathbf{F}\mathbf{b} \otimes \mathbf{a}\Big), \quad (4.6)$$

where $\otimes$ denotes the dyadic product between vectors.

In order to make analytic calculations, we consider the simple case in which the cells initially occupies the domain $\Omega_0 = [0, L] \times [0, L] \times [0, H]$, thus it has a thin geometry with planar square section of width L, and an out-of-plane thickness $H < L$. We also assume that the fibers are initially orthogonal, so that $\mathbf{a} = \mathbf{e}_1$ and $\mathbf{b} = \mathbf{e}_2$. We derive in the following two basic solutions of the elastic boundary value problems representing the two morphologies observed in experiments.

4.2.1. Uniformly compressed solution

By substituting Eq (4.6) into Eqs (4.2,4.3), we search for a uniformly compressed solution, so that the deformation gradient is given by $\mathbf{F} = \lambda \mathbf{I}$, with $\lambda < 1$. We find that λ must be the real root solving :

$$\lambda(\lambda^2 - 1) + \lambda^4 \frac{p_D}{\mu_1} = 0 \quad (4.7)$$

Due to the uniform compression, we remark that $I_8 = 0$, so there is no anisotropic contribution to the stress. The solution of Eq (4.7) is shown in Figure 5 as a function of the dimensionless osmotic stress p_D/μ_1.

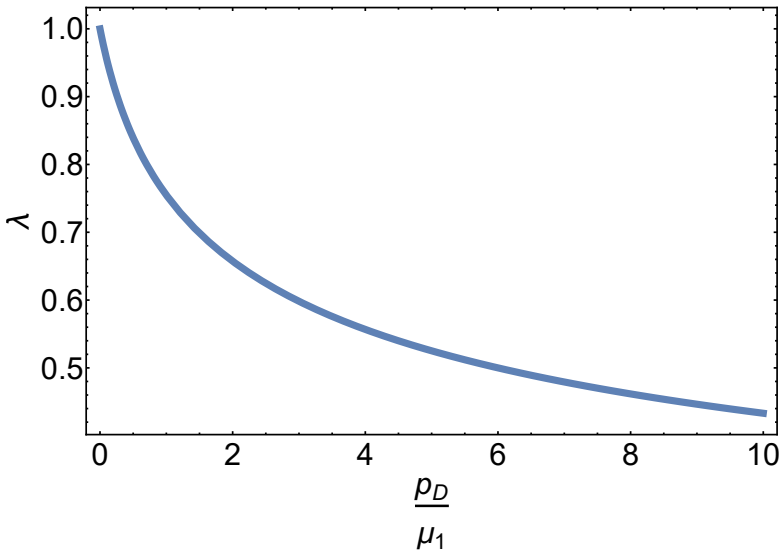

Figure 5. Uniform compressive stretch λ solving Eq (4.7) as a function of the dimensionless osmotic stress p_D/μ_1.

4.2.2. Elongated solution

We search now for an elongated solution of Eqs (4.2,4.3) with the constitutive assumption given by Eq (4.5). Our ansatz for the mapping solution reads:

$$\mathbf{x} = (\alpha X_1 + \delta X_2)\mathbf{e}_1 + \beta X_2 \mathbf{e}_2 + \gamma X_3 \mathbf{e}_3 \tag{4.8}$$

where $\alpha, \beta, \gamma, \delta$ are four unknown parameters.
Substituting Eq (4.8) into Eqs (4.3,4.6), we find the following algebraic system of nonlinear equations:

$$\begin{aligned}
&\delta^2(\mu_1 + \alpha^2\delta^2\mu_2) + \beta^2(\mu_1 - \alpha^2\mu_1 + \alpha^2\delta^2\mu_2) - \alpha\beta^3\gamma p_D - \alpha\beta\gamma\delta^2 p_D = 0\\
&\mu_1 - \beta^2\mu_1 + \alpha^2\delta^2\mu_2 - \alpha\beta\gamma p_D = 0\\
&\mu_1 - \gamma^2\mu_1 + \alpha^2\delta^2\mu_2 - \alpha\beta\gamma p_D = 0\\
&\delta(\mu_1 + \alpha^2\delta^2\mu_2 - \alpha\beta\gamma p_D - 2\alpha^2\beta^2\mu_2 \log(\alpha\beta\gamma)) = 0.
\end{aligned} \tag{4.9}$$

The solution of Eqs (4.9) can be numerically computed using the Newton's methods as a function of the dimensionless osmotic stress p_D/μ_1 at different anisotropy ratios μ_2/μ_1. In particular, we select the solutions such that δ does not vanish, so that the resulting morphology is characterized by a fiber splay causing the elongated shape observed in experiments.

4.3. Results

In this paragraph, we use energetic arguments to identify the onset of a morphology transition between the two basic solutions of the elastic boundary value problem.
For this purpose we write the total mechanical energy E of the system in the spatial configuration as:

$$E = \int_\Omega \Psi d^3\mathbf{x} - p_D(|\Omega| - |\Omega_0|) \tag{4.10}$$

where the first term on the rhs is the total elastic energy within the cell and the second term is the mechanical work performed by the osmotic stress. In the following we use the subscripts c and el to indicate the corresponding values evaluated for the basic solutions given by Eq (4.7) and Eq (4.9) , respectively.

In Figure 6 we depict the total energies of the two basic solution as a function of the dimensionless osmotic stress p_D/μ_1 at a fixed anisotropy ratio $\mu_2/\mu_1 = 0.15$. We find that the uniformly compressed solution has a lower total energy compared to the elongated solution if p_D/μ_1 is lower than a critical value of about 1.2, beyond which the elongated solution is energetically favourable. This means that the cells keeps a symmetric rounded morphology whilst being squeezed by the outer the osmotic pressure, but a topological crossover occurs beyond this critical pressure value towards an elongated shape dictated by the fiber splay. An illustration of the experimental morphologies and the corresponding elastic solutions is depicted in Figure 7.

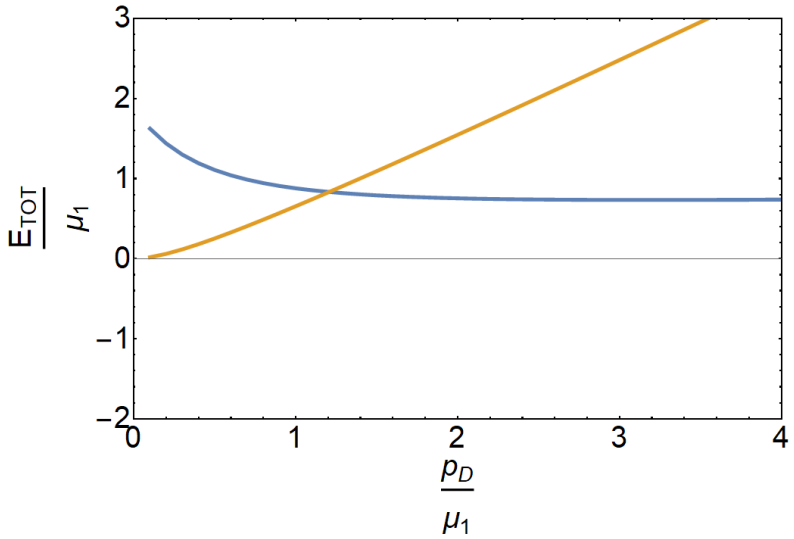

Figure 6. Total dimensionless energies per unit initial volume E_c/μ_1(yellow line) and E_{el}/μ_1 (blue line) of the uniformly compressed and the elongated solutions, respectively, as a function of the dimensionless osmotic stress p_D/μ_1, shown at $\mu_2 = 0.15\mu_1$. The two curves intersect at a critical level $p_{cr} = p_D/\mu_1 = 1.2$.

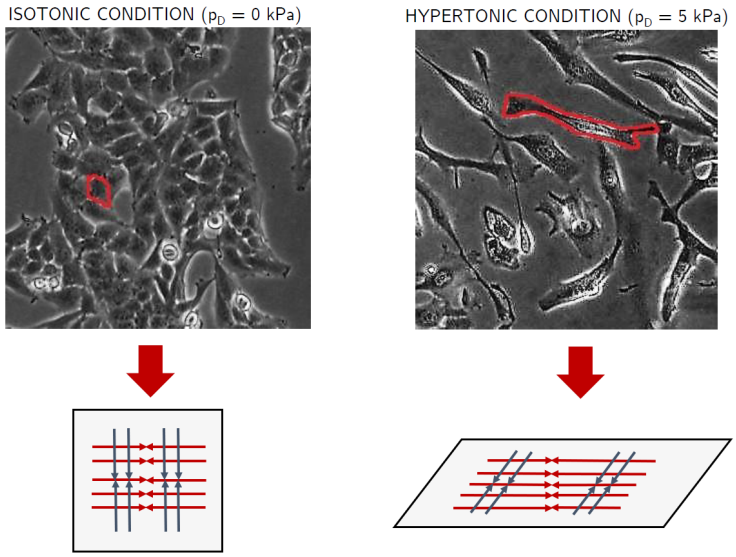

Figure 7. (Top) Zoomed microscopy images showing the red contours of the cells in isotonic (left) and hypertonic (right) conditions. (Bottom) Sketch of the corresponding homogeneous solutions of the elastic boundary problem.

In Figure 8 we depict the critical value $p_{cr} = p_D/\mu_1$ of this morphological crossover as a function of the anisotropy ratio μ_2/μ_1, showing that the critical threshold for the osmotic pressure is of the same order as μ_1 if $\mu_2/\mu_1 = O(1)$. Since for living cells the shear modulus is about $1 - 10$ KPa [32], the critical osmotic pressure is of the same order as the one applied in experiments.

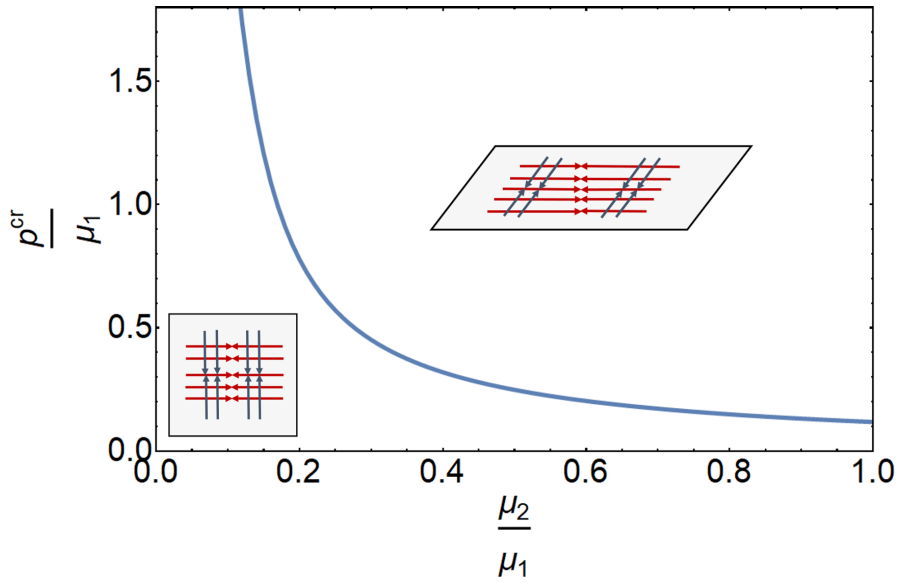

Figure 8. Critical dimensionless threshold p_{cr}/μ_1 of the osmotic stress for the morphological crossover as a function of the dimensionless anisotropic ratio μ_2/μ_1. The region above the curve is characterized by the energetic dominance of the elongated configuration, while the uniformly compressed solution is favoured below.

5. Discussion and concluding remarks

Glioblastoma Multiforme (GBM) is one of the most common and aggressive tumors and practically impossible to treat due to its high invasive and infiltrative growth, despite the great progress made in the last decades for the development of new imaging techniques for brain tumours and for genetic targeting of adjuvant therapies. Our results suggest the micro–environment is a key factor in GBM development owing to the mutual chemo-mechanical feedback exchanged with the tumour. In particular, we have proven new insights on the effect of different osmotic conditions on monolayers made of human glioblastoma cell line (T98G), particularly focusing on the effect on growth and on morphological changes. By means of *in-vitro* experiments, we have shown that the osmotic pressure exerted by a medium rich in Dextran (either 2 or 5 kPa) gives an inhibitory effect on growth compared to the standard isotonic medium. The relative effects on growth and proliferation become more evident at long times, where the majority of living cells flatten and a certain amount of dead cells float in suspension. In both hypertonic and hypotonic cases the results on proliferation were also confirmed by the analysis of the experimental growth curves. Moreover, we correlated the effect of pressure alteration on cell proliferation with the cell cycle progression of Dextran/hypotonic-treated cells. We observed that prolonged culture in hypotonic medium caused an accumulation in G1 phase, which is likely the cause of the observed growth delay; instead, the presence of Dextran in the medium induced an initial accumulation in S phase that definitively resulted in a a G1-phase accumulation at later time. In addition, the analysis of fractional DNA content showed that in presence of high mechanical stress (5 kPa) around 30% of cells did undergo apoptosis. Interestingly, we reported that cells undertake a peculiar elongated morphology in presence of Dextran, in agreement with previous results [15, 17], and they appear more dispersed rather than

gathered in compact clusters. On the contrary, the hypotonic treatment had only a mild effect on growth, without appreciable alteration of the cells morphology.

Thus, we have proposed a mathematical model for the single cell in order to understand the mechanical origin of the morphological transition observed in monolayers in presence of hypertonic stress. Despite the tumour consists in an aggregate of cell, the importance of focusing on the single cell behaviour is due to the need of understanding how the micro-environment can influence the biological processes of the single during the migration process. Considering the time scale of interest (days), the adherent GBM cell is assumed to respond to external solicitation as a solid-like elastic material characterized by the presence in the bulk of an internal micro–structure that accounts for the preferential spatial arrangement of the cytoskeletal fibers, which are assumed to be mainly distributed around two orthogonal directions in the reference configuration. After stating the constitutive law of the strain energy density using the representation theorem of tensor functions, we computed two homogeneous solutions of the nonlinear elastic boundary value problem, corresponding to uniform symmetric compression and elongated shape observed in experiments.
Through energetic considerations we suggested a plausible explanation of the morphology crossover between the two solutions, based on a competition between the isotropic response and the splay contribution given by the cytoskeletal fibers. The theoretical results are in good agreement with the experiments: the uniformly compressed solution is energetic favourable in presence of low osmotic stresses, whilst the elongated solution is dictated by the fiber splay, and it only occurs if the cell is subjected to an osmotic stress beyond a critical threshold, which is of the order of magnitude as the one used in experiments.

Acknowledgments

This work has been supported by the Associazione Italiana per la Ricerca sul Cancro (AIRC) through the MFAG grant 17412 to PC, through IG#18621 to GS, and the Italian Ministry of Health (RF-2013-02358446) to GS. DA acknowledges the MIUR grant ”Dipartimento di Eccellenza 2018-2022” (E11G18000350001).

Conflict of interest

The authors declare no conflict of interest.

References

1. M. Goodenberger and R. Jenkins, Genetics of adult glioma, *Cancer Genet.*, **205** (2012), 613–621.
2. H. Ohgaki and P. Kleihues, The definition of primary and secondary glioblastoma, *Clin. Cancer Res.*, pages clincanres–3002, 2012.
3. D. Orringer, D. Lau, S. Khatri, et al., Extent of resection in patients with glioblastoma: limiting factors, perception of resectability, and effect on survival, *J. Neurosurg.*, **117** (2012), 851–859.
4. B. Mukherjee, B. McEllin, C. V. Camacho, et al., Egfrviii and dna double-strand break repair: a molecular mechanism for radioresistance in glioblastoma. *Cancer Res.*, **69** (2009), 4252–4259.

5. S. Carlsson, S. Brothers and C. Wahlestedt. Emerging treatment strategies for glioblastoma multiforme. *EMBO Mol. Med.*, e201302627, 2014.
6. M. C. Mabray, R. F. Barajas and S. Cha, Modern brain tumor imaging, *Brain Tumor Res. Treat.*, **3** (2015), 8–23.
7. J. Folkman and M. Hochberg, Self-regulation of growth in three dimensions, *J. Exp. Med.*, **138** (1973), 745–753.
8. R. M. Sutherland, Cell and environment interactions in tumor microregions: the multicell spheroid model, *Science*, **240** (1988), 177–184.
9. R. M. Sutherland, J. A. McCredie and W. R. Inch, Growth of multicell spheroids in tissue culture as a model of nodular carcinomas, *J. Natl. Cancer Inst.*, **46** (1971), 113–120.
10. G. Helmlinger, P. Netti, H. Lichtenbeld, et al., Solid stress inhibits the growth of multicellular tumor spheroids, *Nature Biotech.*, **15** (1997), 778.
11. G. Cheng, J. Tse, R. Jain, et al., Micro-environmental mechanical stress controls tumor spheroid size and morphology by suppressing proliferation and inducing apoptosis in cancer cells, *PLoS One*, **4** (2009), e4632.
12. F. Montel, M. Delarue, J. Elgeti, et al., Stress clamp experiments on multicellular tumor spheroids. *Phys. Rev. Lett.*, **107** (2011), 188102.
13. F. Montel, M. Delarue, J. Elgeti, et al., Isotropic stress reduces cell proliferation in tumor spheroids. *New J. Phys.*, **14** (2012), 055008.
14. P. Mascheroni, C. Stigliano, M. Carfagna, et al., Predicting the growth of glioblastoma multiforme spheroids using a multiphase porous media model, *Biomech. Model. Mechanobiol.*, **15** (2016), 1215–1228.
15. B. Bober, J. Love, S. Horton, et al., Actin–myosin network influences morphological response of neuronal cells to altered osmolarity. *Cytoskeleton*, **72** (2015), 193–206.
16. F. Guilak, G. Erickson and H. Ting-Beall, The effects of osmotic stress on the viscoelastic and physical properties of articular chondrocytes, *Biophys. J.*, **82** (2002), 720–727.
17. C. La Porta, A. Ghilardi, M. Pasini, et al., Osmotic stress affects functional properties of human melanoma cell lines, *Eur. Phys. J. Plus*, **130** (2015), 64.
18. A. Taloni, A. A. Alemi, E. Ciusani, et al., Mechanical properties of growing melanocytic nevi and the progression to melanoma. *PloS One*, **9** (2014), e94229.
19. G. Tao, L. Rott, A. Lowe, et al., Hyposmotic stress induces cell growth arrest via proteasome activation and cyclin/cyclin-dependent kinase degradation, *J. Biol. Chem.*, **277** (2002), 19295–19303.
20. M. Delarue, F. Montel, D. Vignjevic, et al., Compressive stress inhibits proliferation in tumor spheroids through a volume limitation, *Biophys. J.*, **107** (2014), 1821–1828.
21. K. Tsujita, T. Takenawa and T. Itoh, Feedback regulation between plasma membrane tension and membrane-bending proteins organizes cell polarity during leading edge formation, *Nature Cell Biol.*, **17** (2015), 749.

22. J. Schindelin, I. Arganda-Carreras, E. Frise, et al., Fiji: an open-source platform for biological-image analysis, *Nat. Methods*, **9** (2012), 676.
23. G. Schmid-Schönbein, K. Sung, H. Tözeren, et al., Passive mechanical properties of human leukocytes, *Biophys. J.*, **36** (1981), 243–256.
24. D. Theret, M. Levesque, M. Sato, et al., The application of a homogeneous half-space model in the analysis of endothelial cell micropipette measurements, *J. Biomechan. Eng.*, **110** (1988), 190–199.
25. R. W. Ogden, *Non-linear elastic deformations*. Courier Corporation, 1997.
26. T. C. Gasser, R. W. Ogden and G. A. Holzapfel, Hyperelastic modelling of arterial layers with distributed collagen fibre orientations, *J. R. Soc. Interface*, **3** (2005), 15–35.
27. A. Agosti, D. Ambrosi and S. Turzi, Strain energy storage and dissipation rate in active cell mechanics, *Phys. Rev. E*, **97** (2018), 052410.
28. R. Rivlin and J. Ericksen, Stress-deformation relations for isotropic materials, *Arch. Ration. Mech. Anal.*, **4** (1955), 323–425.
29. A. Spencer, Part iii. theory of invariants, *Continuum Physics*, **1** (1971), 239–353.
30. D. Ambrosi, S. Pezzuto, D. Riccobelli, et al., Solid tumors are poroelastic solids with a chemo-mechanical feedback on growth, *J. Elasticity*, **129** (2017), 107–124.
31. A. V. Melnik, X. Luo and R. W. Ogden, A generalised structure tensor model for the mixed invariant i8, *Int. J. Non-Lin. Mech.*, **107** (2018), 137–148.
32. C. Lim, E. Zhou and S. Quek, Mechanical models for living cells—a review, *J. Biomech.*, **39** (2006), 195–216.

AIMS Press